Journal of Geography and Geology; Vol. 14, No. 2; 2022
ISSN 1916-9779 E-ISSN 1916-9787
Published by Canadian Center of Science and Education

Recent Transport and Deposition of Littoral Sand Across the Inner-Shelf of Central Oregon: Further Constraints on Estimating Depths of Closure (30–34 m) during Future Sea Level Rise in the Pacific Northwest Region, USA

Curt D. Peterson[1] & Maureen Walczak[2]

[1] Geology Department, Portland State University, Portland, United States

[2] College of Earth, Ocean, and Atmospheric Sciences, Oregon State University, Corvallis, OR., United States

Correspondence: Curt Peterson, Geology Department, Portland State University, Portland, OR., 97207, United States. Tel: 1-503-730-9266. E-mail: curt.d.peterson@gmail.com

The financial support for the collection, documentation, and archival of the vibracores used in this study was provided by the Pacific Marine Energy Center and the Marine and Geology Repository at Oregon State University.

Received: May 2, 2022 Accepted: June 5, 2022 Online Published: June 7, 2022

doi: 10.5539/jgg.v14n2p1 URL: https://doi.org/10.5539/jgg.v14n2p1

Abstract

In this article, geologically recent sedimentation rates across a high wave- and wind-energy inner-shelf are used to constrain depths of closure, which are needed to estimate potential offshore displacements of littoral (beach) sand that could result from future sea level rise (SLR). Seven shallow vibracores (1.0–2.3 m subsurface depth) were analyzed from a single transect across the inner-shelf (19–72 m water depth) at the South PacWave study site in the high-wave energy (peak wave $H_{s=}$ 10–15 m) coast of Central Oregon. The vibracores were ^{14}C dated to establish 1) near-modern mixing depths and 2) net sedimentation rates that equaled or exceeded rates of coeval SLR (10 cm century^{-1}) during very latest-Holocene time (≤1.0 ka). Sedimentation rates of 17 cm century^{-1} and 31 cm century^{-1} for vibracore P1-2A22 in 34 m water depth do exceed coeval SLR, even after accounting for apparent mixing depths of 60–100 cm. But sedimentation rates in deeper core sites (47–53 m water depth) do not approach coeval SLR rates. These results support a proposed near future (one century) 30 m depth of closure in the innermost-shelf of northern Oregon. Vibracore sand grain sizes (mean 0.20±0.03 mm 1σ, n=18) are similar across the inner-shelf, but heavy-mineral sand tracers confirmed that the latest-Holocene inner-shelf sand accumulations were supplied from seaward transport of littoral sand. The net loss of littoral sand to the inner-shelf sand sink accounts for the narrowing and thinning of beach deposits in northern Oregon during latest-Holocene time. A 1.0 m thickness of littoral sand displaced across the innermost-shelf (5–30 m water depth) following a 1.0 m SLR, or equivalent increase in offshore accommodation space, would yield a cross-sectional area of $1.5x10^3$ m^2. That value is three times larger than the mean cross-sectional area of the modern adjacent beaches (mean $4.8x10^2$ m^2) in the South PacWave study area. Following a possible near future SLR of 1.0 m, the popular sandy beaches of northern Oregon could be converted to intertidal gravel/algae covered bedrock platforms.

Keywords: Inner-shelf, sea level rise, accommodation space, littoral sand displacement, beach erosion

1. Introduction

In this article, a single transect of seven vibracores, taken across the inner-shelf at the South PacWave test site in central Oregon (Figure 1), is used to establish a depth of closure (Bruun, 1962) for the last several centuries. Because of the annual high wave- and high wind-energies in this Pacific Northwest (PNW) coastal setting, prolonged sedimentation rates of littoral sand that kept pace with sea level rise (SLR) across the innermost-shelf can be used as proxies for depth of closure for very latest-Holocene time (≤1.0 ka) (Peterson et al., 2020a). Depths of closure are needed to estimate offshore displacements of littoral sand and associated beach sand erosion (Bruun, 1968; Rosen; 1978; Erikson, 2017), which are expected to follow predicted near future SLR

(0.5-1.0 m) from ongoing global warming (Bamber et al., 2019; Horton et al., 2020). The PacWave study area is characterized by high-wave-energy, moderately steep shelf gradient, and relatively low abundance of littoral sand. The inner-shelf vibracores used in this study (PacWave, 2019) are analyzed for 1) texture, 2) sand grain size distributions, 3) unconfined shear strengths, 4) heavy-mineral sand source tracers, and 5) ^{14}C age relations of littoral sand accumulations during very-latest Holocene time. The vibracore records analyzed for this article are compared to previously reported vibralift/vibracore records in other PNW inner-shelf settings that are characterized by large rivers and abundant littoral sand supply (Clifton et al., 1990; Mardock, 1991; Kaminsky, 2006). Recommendations are made for future studies of modern conditions of littoral sand transport across the inner-shelf using long-term monitoring facilities. The approaches used in this study, to constrain depth(s) of closures in the PNW study region, should have direct application to other high-energy inner-shelves worldwide. Such empirical constraints are needed to establish and/or verify inputs to calculations of beach sand erosion following predicted near future SLR (Peterson et al., 2021).

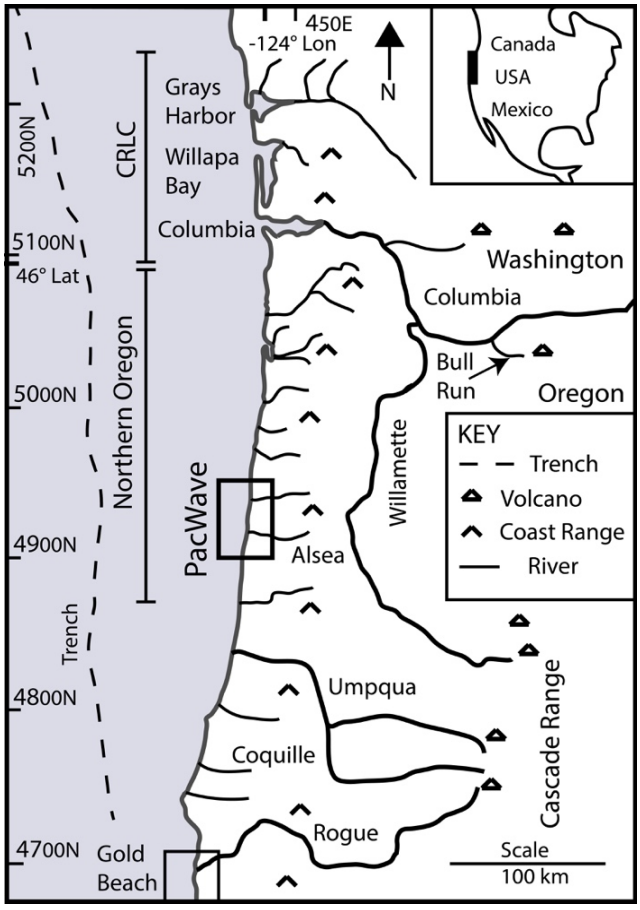

Figure 1. Map of the central part of the Pacific Northwest (PNW) study region

Mapped study region features include 1) the Cascadia subduction zone buried trench, 2) the Cascade volcanic arc, 3) the uplifted Coast Ranges, 4) the large antecedent rivers (named and bold lines) that reach the Cascade volcanic arc, 5) small rivers of the Coast Ranges (not named except for the Alsea and Coquille Rivers), 6) the small Bull Run catchment (Hamilton, 1994), 7) the Northern Oregon subregion (named), 8) the Columbia River Littoral Cell (CRLC), including three large estuaries (Columbia, Willapa Bay and Grays Harbor), 9) the Gold Beach study area (boxed), and 10) the PacWave study area (boxed), which is the subject of this article. UTM coordinates are in meters 10T N.

2. Background

2.1 *Gold Beach, South-central PNW Study Region*

A multi-agency cruise off the southern Oregon coast in the PNW study region (Figure 2A) recovered late-Holocene stratigraphic sections (Figure 2B) by vibralift (4–6 m subsurface depth) from inner-shelf sites located just south of the Rogue River at Gold Beach, Oregon (Clifton et al., 1990). For the purposes of this article, the Oregon inner-shelf of Runge (1966) is divided into the inner-shelf (0–50 m water depth), including

the innermost-shelf (0–30 m water depth), and the mid-shelf (50–100 m water depth). The Gold Beach vibralift sections were recovered from ocean bottom deposits in water depths of 13, 26, 28, and 30 m. The vibralift sites were selected on the bases of 1) surface heavy-mineral concentrations (> 10% wt fractions) and 2) seismic reflection profiles showing undeformed sediments (~6–7 m thickness) above prominent unconformities (Figure 2C) (Clifton et al., 1991). No concentrated heavy-mineral layers or economic placers were observed in the vibralift sand sections (Mardock, 1991), but basal gravel was recovered from the bottom (~6 m subsurface depth) of one site: V3 in 28 m water depth.

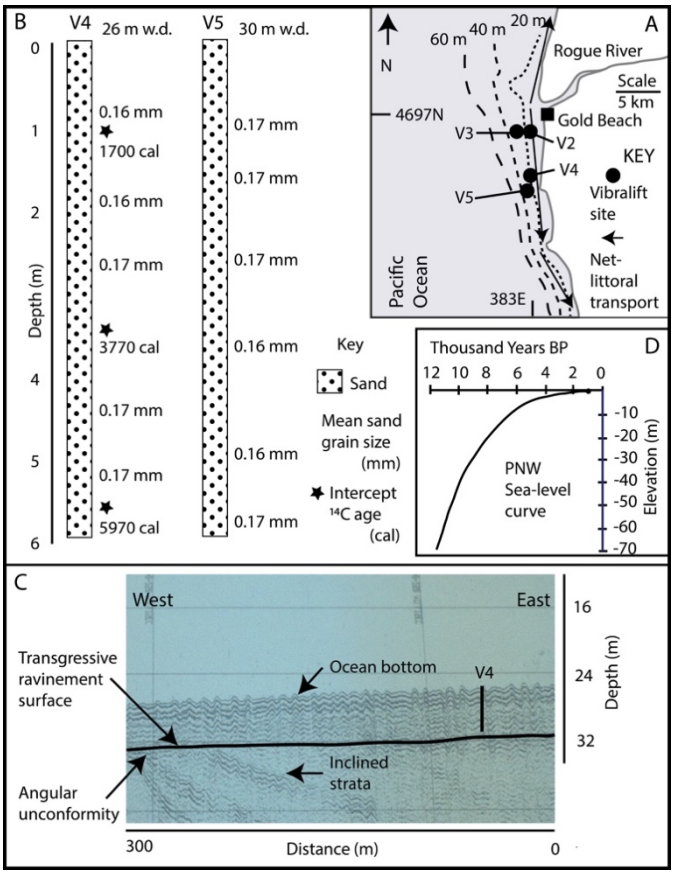

Figure 2. Vibralift sites and stratigraphic sections in the Gold Beach study area

Part A, Mapped study area features include 1) inner-shelf bathymetric contours (m water depth) (dashed lines), 2) vibralift sites, 3) net littoral transport, and 4) the City of Gold Beach at the mouth of the Rogue River. Vibralift sites V4 and V5 coordinates (UTM 10T N), respectively, are 4688350N, 380370E (V4) and 4686790N, 380450E (V5). Part B, Stratigraphic sections are compiled from recovered sample intervals in vibralift sites V4 and V5 (Mardock, 1991). Shell ^{14}C ages (Clifton et al., 1991) were recalibrated in Peterson et al., (2021). Part C, Vibralift site V4 was located on a seismic reflection line, which records 1) an angular unconformity and 2) overlying undeformed deposits of ~6 m in thickness. Vibralift site V5 was located ~1.5 km south of the seismic line. Part D, Relative sea-level curve for the PNW region (Peterson et al., 2016).

Shell ^{14}C analyses from vibralift site V4 yielded calibrated intercept ages of 1700, 3700, and 5970 cal, respectively at subsurface depths of 1.0 m, 3.7 m, and 6.1 m (Figure 2B) (Clifton et al., 1991; Peterson et al., 2021). The recovered vibralift sections were interpreted as late-Holocene sand (fill) over a transgressive ravinement surface (Figure 2C). It was not established whether the Holocene ravinement surface reoccupied an older (previously cut) ravinement surface. The apparent Holocene ravinement surface in 32 m water depth in the vicinity of site V4 correlates to a sea level position at 9 ka (Figure 2D), leaving a ~3 ka age gap between the overlying sand (≤6 ka) and the underlying ravinement surface. Importantly, the hypersthene-rich sand mineralogy in site V4 (Peterson et al., 2021) demonstrates that the sand fill was derived from adjacent beaches, ultimately sourced by the large Rogue River. The inner-shelf sand deposits in the Gold Beach study area represent seaward transport and deposition of littoral sand across the innermost-shelf to at least 30 m water depth during late-Holocene time. The middle ^{14}C age at 3.7 ka in site V4 yields a sedimentation rate of 1.0 ka yr^{-1}, which is equivalent to the coeval rate of regional net sea level rise and increasing accommodation space (~1.0 m

ka^{-1}) across the inner-shelf (Peterson et al., 2019). Extending similar fill rates to nearby site V5 (Figure 2A) in 30 m water depth, suggests a ≥30 m depth of closure for latest-Holocene time (3–0 ka). Is this depth of closure appropriate for other inner-shelf localities in the PNW study region? The Gold Beach study area in the southern PNW study region is characterized by 1) proximity to the large Rogue River (bedload throughput ~$0.7x10^6$ m^3 yr^{-1}), 2) dominant southward littoral transport, 3) converging/diverging inner-shelf contours, and 4) moderately steep inner-shelf gradients of ~1.0% (Figure 2A) (Peterson et al., 2009; Peterson et al., 2021). Examples of depths(s) of closure in a low-gradient (broad) inner-shelf setting of the Columbia River Littoral Cell (CRLC) in the northern PNW study region (Figure 1) are presented below.

2.2 Columbia River Littoral Cell, North-central PNW Study Region

Catastrophic beach retreat scarps resulted from episodic coseismic subsidence events in the large CRLC (160 km length) in the northern PNW study region (Figure 3A) (Meyers et al., 1996; Woxell, 1998). The retreat scarps (~1% bottom gradients) are identified by basal heavy-mineral placers (landward) and basal shell/pebble lags below inclined beach laminae (seaward), as recorded in GPR profiles and auger borehole/vibracore logs. The last coseismic subsidence event (1700 CE) produced 1.0–1.5 m of abrupt SLR across the inner-shelf, which resulted in at least 400 m of beach retreat in profile WARR1R1 (Figure 3B). Similar preserved retreat scarps from the 1700 event, reaching ~400–500 m in across-shore extents, occur at OHYU1R1 and 116th, located respectively north and south of WARR1R1 (Fig), as well as at other profile locations in the CRLC subcells (Peterson et al., 2002; Peterson et al., 2010). The catastrophic beach retreats occurred in response to the displacements of beach sand across the broad inner-shelf and to large marine dominated estuaries in the CRLC system, following the coseismic subsidence and corresponding SLR of 1.0–1.5 m in 1700.

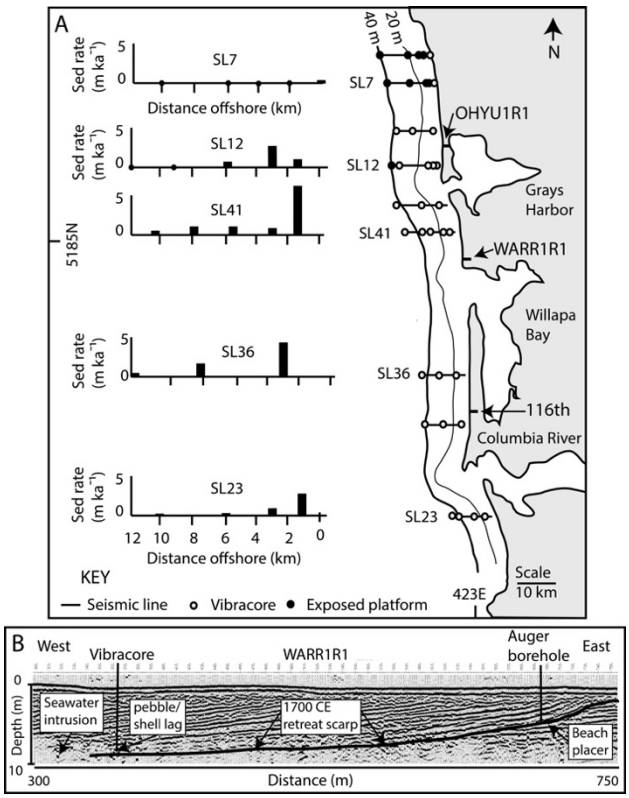

Figure 3. Map, sedimentation rates, and catastrophic beach retreat scarp in the Columbia River Littoral Cell (CRLC)

Part A, Mapped study area features include: three large estuaries (Columbia River, Willapa Bay, and Grays Harbor), inner-shelf bathymetric contours (m), seismic lines (SL) (Twichell et al., 2010), vibracore and exposed bedrock platforms sites (circles) (Kaminsky, 2006), and corresponding latest-Holocene (3–0 ka) sedimentation rates (Peterson 2020b). Three representative ground penetrating radar (GPR) profiles are numbered (OHYU1R1, WARR1R1, and 116th). Part B, GPR profile (WARR1R1) showing 1700 CE catastrophic beach retreat scarp (> 400 m length). Seawater intrusion precluded signal penetration in the modern beach backshore and foredune, ~300 m west of the displayed profile segment (Peterson et al., 2020b).

The onset of beach recovery (~1770 CE) in the Grayland Plains subcell was established by ^{14}C dating of reactivated foredune deposition adjacent to the WARR1R1 profile (Figure 3) (Peterson et al., 2020b), thereby constraining the period of offshore displacement of beach sand to < 70 years. Northward migration of the Willapa Bay tidal inlet is now threatening the WARR1R1 profile, but in 1700 the tidal inlet was located ≥3.0 km south of its present position (Woxell, 1998). The earliest return of the displaced beach sand to the eroded CRLC beaches, following the 1700 coseismic subsidence, is assumed to coincide with the initial phase of interseismic uplift across the inner-shelf (Cruikshank and Peterson, 2017). During the following 100 years (~1770–1870) of interseismic uplift, and the continued return of displaced beach sand from the inner-shelf, the shoreline progradation adjacent to WARR1R1 averaged 2.3 m yr^{-1}, as modified from Woxell (1998). Even though interseismic uplift declined, the rate of shoreline progradation for the early- and middle- historic period of 1870–1995 increased to 5.4 m yr^{-1}. Some of the early-historic increase in progradation rate is attributed to throughput of Columbia River bedload to the marine side. Throughput of Columbia River sand to the littoral zone likely increased well above natural rates due to widespread farming/grazing, clear-cut logging, and earthmoving construction in the early 1900s. For example, in a western Cascade Range drainage basin (Bull Run, Oregon) (Figure 1) an impoundment (dam) catchment recorded a ~3x increase in sedimentation rates after the onset of clear-cut logging and road building in the drainage basin (Hamilton, 1994). Some beaches that are adjacent to the Columbia and Grays Harbor estuary mouths are reported to have prograded following jetty construction and ebb tidal delta alterations in the early 1900s (Kaminsky, et al., 2010). The development of Columbia River tributary impoundments during the 1960s–1970s (Sherwood, et al., 1990) likely reduced river bedload supplies, though modern rates of Columbia River sand throughput to marine side are not directly established. Of importance to this paper, the anomalously high progradation rates of CRLC barriers and beach plains in the early 1900s both preserved the buried 1700 retreat scarps and restricted seawater intrusion, which prohibits GPR signal penetration (Figure 3B).

Offshore vibracoring in the CRLC system (Figure 3A) (Kaminsky, 2006) shows geologically recent transport and accumulation of Columbia River-sourced littoral sand (Twichell et al., 2010) across the inner-shelf, where offshore bottom gradients exceed ~0.4%. The ^{14}C dated vibracores record significant transports of littoral sand across the innermost-shelf to reach water depths of 30–40 m, or 5–8 km distances offshore in latest-Holocene time. The largest sedimentation rates in the innermost-shelf reflect upper-shoreface progradation, preceding progradation of beach plains and barrier spits. Interpretations of modern depths of closures in the CRLC system (Peterson et al., 2020b) are based on multiple dated core intervals of very-latest Holocene time (≤1.0 ka) from similar water depths, which yielded sedimentation rates that equal or exceed the coeval rates of net SLR (~1.0 m ka^{-1}). In the CRLC a 30 m depth of closure is predicted for one meter of SLR over a one century period. However, the CRLC is characterized by unusual conditions of 1) very-large river sand supplies (2– $3x10^6$ m^3 yr^{-1}), 2) ebb tidal delta projections to 40 m water depth, 3) shallow inner-shelf gradients (0.35–0.59%), 4) large magnitudes of episodic coseismic subsidence (1±0.5 m), and 5) complex interactions between Columbia River sand throughput and partitioning into the inner-shelf, large estuaries, and prograding beach plains and barrier spits (Peterson et al., 2020b). A search was undertaken to identify less complex coastal settings in the central PNW region where representative depths of closures could be established for those less complex littoral systems, as addressed below.

2.3 Northern Oregon Coast and Inner-shelf, Central PNW Study Region

Much like the CRLC study area to the north, the northern Oregon coast (Figure 4) is characterized by high wave-energy (peak H_s 10–15 m), strong onshore storm winds (sustained winds ≥8 m s^{-1}), and meso-tidal ranges (~3.0 m) (Peterson et al., 2020a). But unlike the large CRLC system, the northern Oregon coast is divided into short subcells (8–25.5 km length) by rocky headlands. The subcells contain narrow beaches (110 ±50 m 1σ width, n=47) and small intervening estuaries or river mouths (Peterson and Kingen, 2021). The magnitude of coseismic subsidence in the northern Oregon coast diminishes from north (~1.0 m) to south (<0.5 m) due to an interception of the Cascadia subduction zone 1st zero-isobase of upper-plate flexure (Peterson et al., 2000), as shown in Figure 4.

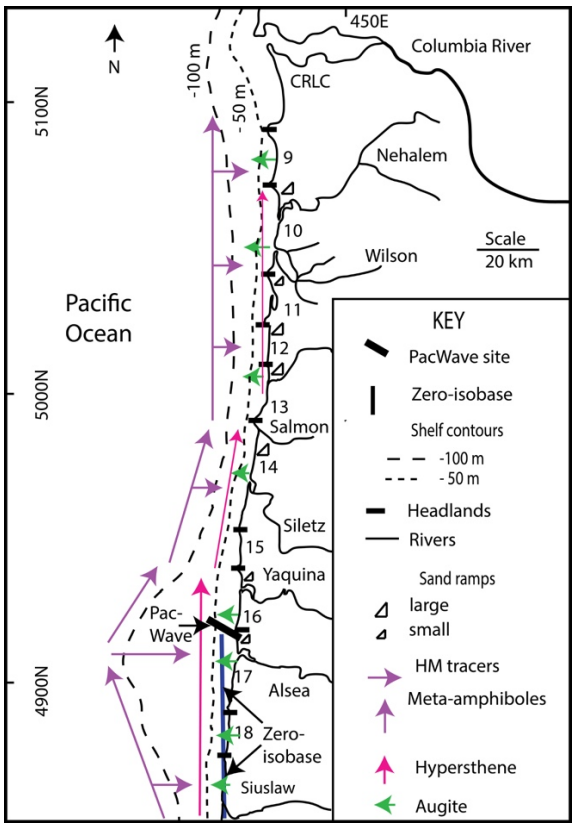

Figure 4. Map of Northern Oregon coastal features

Mapped study area features include 1) PacWave study site, 2) 1st zero-isobase of upper-plate megafold (bold line), 3) shelf bathymetric contours (dashed lines) in meters, 4) rivers (lines), 5) subcell dividing headlands (bars) and associated subcells (numbered), 6) major late-Holocene sand ramps (triangles), and 7) heavy-mineral (HM) sand source tracers including metamorphic amphiboles, hypersthene, and augite. Tracer arrows show end-member component dispersals (Scheidegger et al., 1971) and interpreted transport directions (Peterson et al., 2020a; Peterson et al., 2021). Full extent of Columbia River Littoral Cell (CRLC) is shown in Figures 1 and 2.

The northern Oregon inner-shelf (Figure 4) demonstrates seaward transport of littoral sand to ~ 50 m water depth, as based on inner-shelf sand deposit mineralogy (Figure 4) (Scheidegger et al., 1971). The shelf sand deposits in PNW region contain mixtures of three end-member components or sources of heavy-minerals. The timing and directions of sand supply are interpreted below, following Peterson et al. (2020a) and Peterson et al. (2021). Outer-shelf sand, which is enriched in metamorphic amphiboles, is thought to represent low-stand northward transport in late-Pleistocene time (Scheidegger et al., 1971). Some of the outer-shelf sand was transported across-the shelf by eolian processes during latest-Pleistocene low-stand conditions (Peterson et al., 2007). The mid-shelf dune sheets were eroded and remobilized (transported) across the mid-and inner-shelf by asymmetrical wave transport during the Holocene marine transgression. Littoral sand, which was admixed with augite-rich local river sand during the late-Holocene near high-stand, is thought to have been transported seaward across the innermost-shelf in latest-Holocene time (Peterson et al, 2020a). The shelf sand distributions in northern Oregon (Figure 4) are complicated by a third component, hypersthene, which is derived from the large antecedent Umpqua River, located south of the central Oregon study area (Figure 1). The hypersthene component locally extends northward from the southern end of the study area mid-shelf, indicating net-northward sand transport during Holocene time. Of importance to this article, the ages and sedimentation rates of littoral sand supplies, which were transported offshore (seaward) across the inner-shelf in latest-Holocene time, have been used as proxies for future sand displacements to the offshore following predicted future SLR. However, those rates were not directly established in northern Oregon by Peterson et al. (2020a) and were only tentatively constrained in the preliminary study of the PacWave study area (Peterson et al., 2021), as presented below in Section 2.4.

Apparent net northward transport of littoral sand along the northern Oregon coast during late-Holocene time is demonstrated by sand ramps at the northern ends of the headland-bounded subcells (Figure 4) (Peterson et al., 2009). Over short time scales, such net northward longshore transport might not have been significant. But at

millennial time scales, the north-bounded sand ramps became prominent, increasing from maximum elevations of ~25 m in the southern subcells (16 and 17) to ~100 m in the northern subcells (14, 13, 12, and 10). In latest-Holocene (3–0 ka) time, the apparent net longshore transport throughout the northern Oregon beaches has apparently declined relative to offshore transport, as most of the north-bounded sand ramps show ongoing evidence of basal truncation by winter storm surf (Peterson et al., 2019; Peterson et al., 2020a).

2.4 PacWave Study Area in the Northern Oregon Coast

A transect of the inner-shelf of north-central Oregon (Figure 5A) was recently vibracored, prior to intended installations of experimental wave-energy equipment (PacWave, 2019). The study site, identified as the South PacWave site (PacWave, 2022), is located between the mouths of the Yaquina Bay and Alsea Bay estuaries. The shallow stratigraphies of the vibracores (0.5–2.3 m depth subsurface) recovered at the South PacWave site are the subjects of this article. Jetties have been developed at the mouth of Yaquina Bay. Dredge spoils from the bay mouth have been disposed at several sites, located offshore of the jetties, from 1919 to the present (USACE, 2015). No jetties were developed at the mouth of Alsea Bay, so no dredge spoil disposal has occurred offshore of the Alsea Bay mouth. Considering the weak net northward littoral transport in the PacWave study area (subcells 16 and 17) (Figure 4), no impacts from jetty construction and/or disposal of dredge spoils offshore of the Yaquina Bay jetties should have impacted the South PacWave site. Ebb tidal deltas reach less than ~10 m water depth at the mouths of the small Yaquina and Alsea Bays, so they are not thought to have significantly influenced inner-shelf sand transport. Estimated river bedload supplies to Yaquina Bay ($13x10^3$ m^3 yr^{-1}) and Alsea Bay ($25x10^3$ m^3 yr^{-1}) are relatively small (Peterson et al., 2021). Throughput of river sand to the marine side is further reduced by some river sand trapping in the shallow Yaquina Bay (Kulm and Byrne, 1966) and Alsea Bay (Peterson et al., 1982).

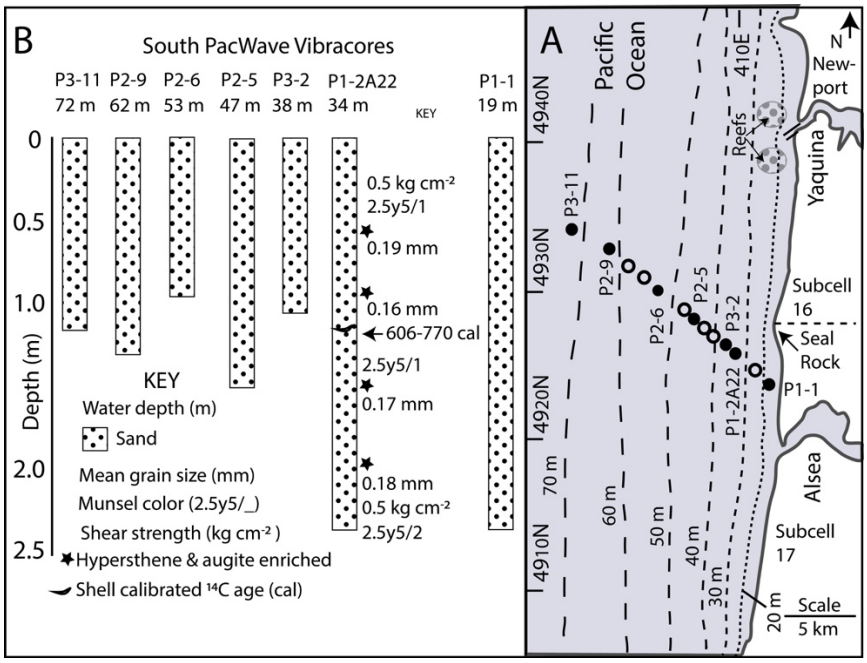

Figure 5. Map of PacWave study area and preliminary vibracore logs

Part A, PacWave study area features include 1) subcells 16 and 17, as divided by the small Seal Rock headland, 2) Yaquina and Alsea Bays, 3) shelf bathymetric contours (20–70 m water depth), and 4) the South PacWave vibracore sites (circles) including those addressed in this article (solid circles). Shallow rocky reefs (15–30 m water depths) occur on either side of the Yaquina Bay harbor entrance (stippled pattern). Inner-shelf bathymetry is from Google Earth (2022). Part B, Preliminary logs are shown from the representative vibracores that are addressed in this article. One vibracore (P1-2A22) was analyzed for sand source(s) and ^{14}C age (Peterson et al, 2021).

The beach shorelines in the PacWave study area (Figure 5A) are uniformly orientated north south. The two subcells are partially separated by a small headland, Seal Rock, composed of resistant basalt, which projects only ~300 m seaward of the adjacent shorelines. Representative beach sand grain sizes (summer beach face) from adjacent modern beaches are 0.16 ±0.02 mm 1σ diameter, n=11 (Peterson and Kingen, 2021). Five representative beaches were sampled during the winter (mid-beach face) and yielded slightly larger mean grain

sizes of 0.22±0.02 mm 1σ diameter, n=5. Modern beach widths in the PacWave study area are 128 ±41 m 1σ width, n=11. The shallow beach sand (1–5 m thickness) that fronts the low sea cliffs overlies thin basal gravel layers (sandstone and basalt pebbles/cobbles) above bedrock beach platforms. The low sea cliffs (7±6 m 1σ m in height n=21) (Peterson et al., 2021) are composed of tertiary sedimentary rocks and overlying marine terrace deposits and/or late-Pleistocene dune deposits (Priest and Allan, 2004). The inner-shelf bathymetric contours in the PacWave study area are parallel to the beach shorelines. The inner-shelf bathymetric contours show no significant divergence or convergence alongshore (Figure 5A). Inner-shelf bottom gradients from 0 m to 30 m water depths in the PacWave study area are 1.2 ±0.2% 1σ, n=8 (Peterson and Kingen, 2021). The innermost-shelf gradient (0–30 m water depth) at the South PacWave study site is 1.4%. Mean sand grain sizes of inner-shelf surface deposits (100% sand) in the PacWave study area are relatively uniform as follows: mean=0.190 mm, n=4 (10–30 m water depth) and mean=0.193 mm, n=4 (30–50 m water depth) (Runge, 1966).

Due to the proximity of the Cascadia 1st zero-isobase to the PacWave study area (Figure 4), most of the events of subduction zone coseismic subsidence area are thought to fall within 0.5–1.0 m coastal submergence or corresponding abrupt SLR. However, the coseismic subsidence records from the last Cascadia megathrust rupture (1700 CE) in the westernmost tidal marshes in Yaquina Bay and Alsea Bay (Figure 5A) indicate <0.5 m subsidence (Peterson et al., 2000). The paleotsunami runup from the 1700 event was modest (~7 m) in the South PacWave site (Peterson et al., 2015). The next oldest Cascadia megathrust rupture that crossed through the PacWave study area occurred in 1,100 cal.

The narrow beaches in the PacWave study area (Figure 5A), and throughout most of Northern Oregon (Figure 4), show abundant evidence of latest-Holocene narrowing and/or thinning, as based on exposures of late-Holocene beach platform stumps (Hart and Peterson, 2007) and truncated sand ramps (Peterson et al., 2019). The modest supplies of beach sand from 1) eroding sea cliffs, 2) river/creek throughputs, and/or 3) northward long-shore transport, over millennial time scales, were unable to maintain beach sand volumes during latest-Holocene time (≤3.0 ka). It has been proposed that the innermost-shelf has served as a major sink for the eroded beach sand in the northern Oregon coast, including the PacWave study area, during that time.

The South PacWave project performed shallow vibracoring (0.5–2.5 m subsurface depth) across the inner-shelf (Figure 5A) to establish sea bottom conditions for securing wave-energy research equipment (PacWave, 2019). The vibracores became available for study by these investigators in 2020 and were found to be dominated by fine sand (Figure 5B). One vibracore, P1-2A22 from 34 m water depth, was analyzed for its source of sand and a representative (mid-core depth) age. Vibracore P1-2A22 yielded littoral-sourced sand to 2.3 m subsurface depth and a shell ^{14}C age of 606–770 cal at 118 cm depth subsurface (Peterson et al., 2021). Detailed analyses and interpretations of the selected South PacWave vibracores are presented below in Section 4.

3. Methods

The South PacWave vibracores (7 cm in diameter) were collected in 2019 and archived in the Marine Geology Repository at Oregon State University under the ISGN index OSU-MSL1903. South PacWave vibracores used for this article (Figure 5 and Table 1) were selected for detailed study based on 1) maximum available core lengths and 2) approximately even spacing between vibracore water depths. Core logging included 1) dominant deposit texture (sand, mud, and lag) under 10x magnification using an American/Canadian Stratigraphic™ grain size card, 2) unconfined shear strength (kg cm^{-2}) using penetrometer resistance, and 3) sediment moist color by Munsell color chart. Selected samples were analyzed for 1) sand grain size (mm) under microscopy (250x) using a calibrated optical micrometer (100 grain count) and 2) relative abundances of source (tracer) heavy-minerals (Scheidegger et al., 1971; Peterson et al., 2020a), including augite, hypersthene, and metamorphic amphiboles, under petrographic microscopy at 250x magnification (100 grain count). Pebbles were measured for intermediate diameter (mm). Samples of shell and wood were collected for AMS ^{14}C analysis. Some shell/wood samples can lead to anomalous ages in inner-shelf settings that are characterized by high wave-energy and low sedimentation rates. In this study small disarticulated (separate) bivalve fragments (~0.5 g) were selected for ^{14}C age analyses. However, anomalous ages could occur from shell fragment remobilization and mixing during high-energy hydrodynamic events. AMS sample pretreatments, isotope analysis, and age calibrations were completed by Beta Analytic Inc (https://www.radiocarbon.com).

Table 1. Vibracore data for the South PacWave site

Core site	UTM-E (m)	UTM-N (m)	Water depth (m)	Core length (cm)	Offshore distance (m)
P1-1	412269	4924646	19	229.5	1,593
P1-2A22	411119	4925483	34	231	2,743
P3-2	410822	4925899	38	110	3,040
P2-5	407220	4928760	47	145	6,642
P2-6	406285	4929540	53	97.5	7,577
P2-9	403668	4931556	62	129	10,194
P3-11	401756	4932874	72	111.5	12,106

Notes: South PacWave vibracores and core sites (Core site) are assigned ISGN index OSU-MSL1903. Selected core site positions (n=7) are presented in UTM (m). Water depth (m) is presented as reported from recovery. Core length is presented as reported from archival. Offshore distance is estimated from the shoreline position (UTM-E 413862, UTM-N 4924646) located due east of P1-1 at the southern end of the diagonal vibracore transect (Figure 5).

4. Results

4.1 South PacWave Vibracore Descriptions

The South PacWave vibracores (Figure 5) were logged for detailed analyses of texture, unconfined shear strength, color, and representative sand grain sizes at 10 cm intervals down core (Table 2). The log data are summarized in Figure 6. The dominant texture in all cores is sand (sand ~100% weight percent), which generally falls into either fine upper (0.177–0.250 mm) or fine lower (0.125–0.177 mm) size classes (Figure 7A). Erosional lag layers (1–2 cm in thickness) are uncommon but include slightly coarser sand, shell fragments, and generally small pebbles (<1.0 cm diameter). Only three lag layers reach greater thicknesses (> 5 cm). They are located at 1) 10–18 cm depth in P1-1 and 2) 0–10 cm depth and 70–82 cm depth in P1-2A22 (Figure 7B). One large pebble (2.5 cm diameter) occurred at 10 cm core depth in P1-1 from 19 m water depth. Small pebbles were not observed in interpreted lag layers from vibracores in sites deeper than 34 m water depth. The shell fragments in lag layers are in sand matrix support (inclined orientation), indicating sandy-lag transport by sheet (fluidized) sand flow. Two rare sandy-mud layers occur at 18–27 cm depth in P2-9 and at 24–40 cm depth in P3-11 (Figure 7E). Representative sand grain sizes were relatively similar in all the vibracores, generally ranging from 0.16±0.03 mm to 0.22±0.6 mm in diameter (Table 2, Figure 6). Sand sizes decreased in the two sandy-mud layers in vibracores P2-9 (0.12±0.7 mm at 20 cm depth) and P3-11 (0.07±0.03 mm at 30 cm depth). The top contacts of the sandy-mud layers in P2-9 and P3-11were disturbed, possibly during vibracoring. The relatively short lengths (≤ 110 cm) of penetration/recovery in core sites 92-5, P2-6, P2-9, and P3-11 are attributed to greater sand compaction (unconfined shear strength ≥ 1.5 kg cm^{-2}) in those sites, as reported below.

Table 2. Core log data for selected vibracores in the South PacWave study site

Core/ cm	Texture	Shear kg cm^{-2}	Color	Sand size mm	Core/ cm	Texture	Shear kg cm^{-2}	Color	Sand size mm
P1-1					80	fU	<0.25	2.5Y 6/1	
0	fU	<0.25	2.5Y 6/1	0.20±0.5	90	fU	<0.25	2.5Y 6/1	
10	Lag	<0.25	2.5Y 6/1		100	fU	<0.25	2.5Y 5/1	0.17±0.04
20	fU	<0.25	2.5Y 6/1		110	fU	<0.25	2.5Y 5/1	
30	fU	<0.25	2.5Y 5/1		P2-5				
40	fU	<0.25	2.5Y 6/1		0	fU	0.25	2.5Y 5/1	
50	fU	<0.25	2.5 Y 6/1	0.22±0.6	10	fU	0.25	2.5Y 5/1	0.18±0.04
60	fU	<0.25	2.5 Y 6/1		20	fU	0.25	2.5Y 5/1	
70	fU	<0.25	2.5 Y 6/1		30	fU	0.25	2.5Y 5/1	
80	fU	<0.25	2.5 Y 6/1		40	fU	0.5	2.5Y 5/1	
90	fU	<0.25	2.5 Y 6/1		50	fU	0.5	2.5Y 5/1	0.19±0.05
100	fU	<0.25	2.5 Y 6/1	0.19±0.04	60	fU	1	2.5Y 5/1	
110	fU	<0.25	2.5 Y 6/1		70	fU	1	2.5Y 5/1	
120	fU	<0.25	2.5Y 5/1		80	fU	1.5	2.5Y 5/1	
130	fU	<0.25	2.5Y 6/1		90	fU	1	2.5Y 5/1	
140	fU	<0.25	2.5Y 6/1	0.21±0.05	100	fU	1.5	2.5Y 5/1	0.23±0.07
150	fU	<0.25	2.5Y 6/1		110	fU	1.25	2.5Y 5/1	
160	fU	<0.25	2.5Y 6/1		120	fL	1.5	2.5Y 5/1	
170	fU	<0.25	2.5Y 6/1		130	fU	1.5	2.5Y 5/1	
180	fU	<0.25	2.5Y 6/1		140	fU	1.5	2.5Y 5/1	
190	fU	<0.25	2.5Y 6/1		P2-6				
200	fU	<0.25	2.5Y 6/1		0	fU	0.5	2.5Y 5/1	0.21±0.06
210	fU	<0.25	2.5Y 6/1		10	fU	0.5	2.5Y 5/1	
220	fU	<0.25	2.5Y 6/1		20	fU	0.5	2.5Y 5/1	
P1-2A22					30	fU	0.75	2.5Y 5/1	
0	Lag	<0.25	2.5Y 5/1		40	fU	0.75	2.5Y 5/1	
10	FU	0.25	2.5Y 5/1		50	fU	0.75	2.5Y 5/1	0.19±0.05
20	fU	<0.25	2.5Y 5/1		60	fU	0.75	2.5Y 5/1	
30	fU	<0.25	2.5Y 5/1		70	mL	1.5	2.5Y 5/1	0.28±0.07
40	fU	<0.25	2.5Y 5/1		80	mL	0.75	2.5Y 5/1	
50	fU	<0.25	2.5Y 5/1	0.19±00.5	90	fU	0.75	2.5Y 5/1	0.19±0.06
60	fU	<0.25	2.5Y 5/1		100	fU	1	2.5Y 5/1	
70	Lag	<0.25	2.5Y 5/1		P2-9				

80	fU	0.25	2.5Y 5/1		0	fU	0.5	2.5Y 6/1	0.19±0.06
90	fU	0.25	2.5Y 5/1		10	fU	0.5	2.5Y 6/1	0.18±0.06
100	fU	0.25	2.5Y 5/1	0.16±0.03	20	Mud	2.25	2.5Y 4/1	0.12±0.7
110	fU	0.25	2.5Y 5/1		30	fL	2.5	2.5Y 4/1	
120	fU	<0.25	2.5Y 5/1		40	fL	3	2.5Y 5/1	
130	fU	<0.25	2.5Y 5/1		50	fL	2.5	2.5Y 5/1	
140	fU	<0.25	2.5Y 5/1		60	fL	3	2.5Y 5/1	
150	fU	<0.25	2.5Y 5/1	0.17±0.04	70	fL	3	2.5Y 4/1	
160	fU	<0.25	2.5Y 5/1		80	fU	3	2.5Y 4/1	
170	fU	<0.25	2.5Y 5/1		90	fL	2.5	2.5Y 5/1	0.17±0.05
180	fU	<0.25	2.5Y 5/1		100	fU	2.5	2.5Y 5/1	
190	fU	<0.25	2.5Y 5/1		110	fL	2.5	2.5Y 5/1	
200	fU	<0.25	2.5Y 5/1	0.18±0.04	P3-11				
210	fU	<0.25	2.5Y 5/1		0	fU	0.5	2.5Y 5/1	0.20±0.07
220	fU	<0.25	2.5Y 5/1		10	fU	0.5	2.5Y 5/1	0.21±0.09
230	fU	<0.25	2.5Y 5/1		20	Mud	0.75	2.5Y 4/1	
P3-2					30	Mud	1.5	2.5Y 3/1	0.07±0.03
0	fU	<0.25	2.5Y 5/1		40	fL	2.5	2.5Y 4/2	
10	fU	<0.25	2.5Y 5/1	0.18±06	50	fU	2.5	2.5Y 5/1	0.18±0.03
20	fU	<0.25	2.5Y 5/1		60	fL	2.5	2.5Y 5/1	
30	fU	<0.25	2.5Y 5/1		70	fL	1.5	2.5Y 5/1	0.17±0.05
40	fU	<0.25	2.5Y 5/1		80	fL	2	2.5Y 5/1	
50	fU	<0.25	2.5Y 5/1	0.19±0.05	90	fU	1.5	2.5Y 5/1	
60	fU	<0.25	2.5Y 5/1		100	fL	1.5	2.5Y 4/2	
70	fU	<0.25	2.5Y 6/1		110	fU	1.5	2.5Y 5/1	

Notes. Cores include number and subsurface depths (cm). Texture includes dominant grain size from grain-size card under microscopy including 1) dominant sand, designated as fine lower (fL) 0.125–0.177 μm, fine upper (fU) 0.177–0.250 mm and, medium lower (mL) 0.250–0.350 mm, 2) sandy-mud (Mud), and 3) lag (Lag) of sand, shell fragments, and small pebbles < 1.0 cm. Unconfined shear strengths (Shear) are from pocket penetrometer (kg cm^{-2}). Moist colors (Color) are from Munsell color charts. Sand mean grain sizes (Sand size) (mean±1 std dev) are in millimeters (mm), measured under microscopy (250x) with calibrated micrometer. See Table 1 for vibracore positions and corresponding water depths in the inner-shelf of the South PacWave study site.

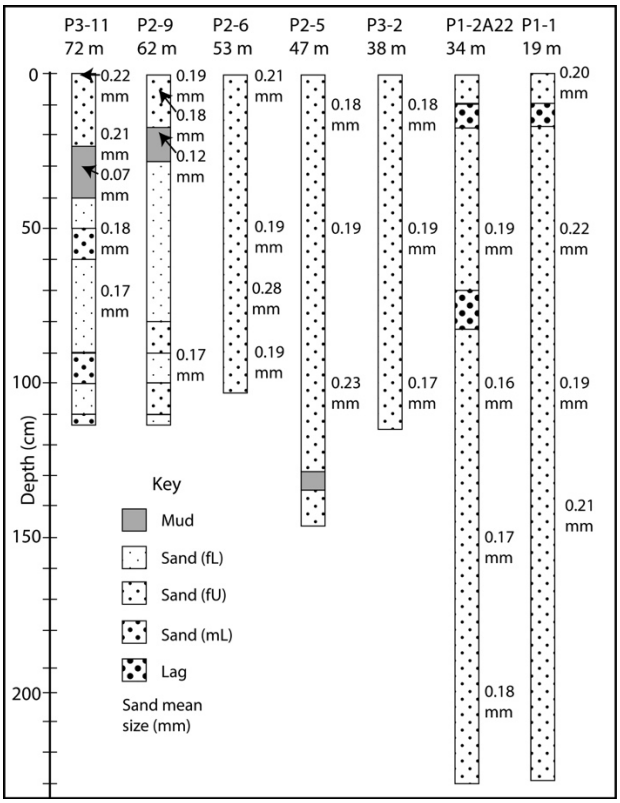

Figure 6. Textures of South PacWave vibracore deposits

Textures and sand mean grain sizes (mm) of South PacWave vibracore deposits are from Table 2. Sand textures include fine lower (fL=0.125–0.177 mm), fine upper (fU=0.177–0.250 mm), and medium lower (mL=0.225–0.350 mm). Sandy mud texture is less than 50% sand. Lag texture generally includes sand, shell fragments, and small pebbles (<1.0 cm), with the shells and pebbles in sand matrix support (see selected core photographs in Figure 7). See Figure 5 for locations of the vibracore sites in the PacWave study area. Radiocarbon dating results from selected vibracore sections are provided in Table 4 of Section 4.4.

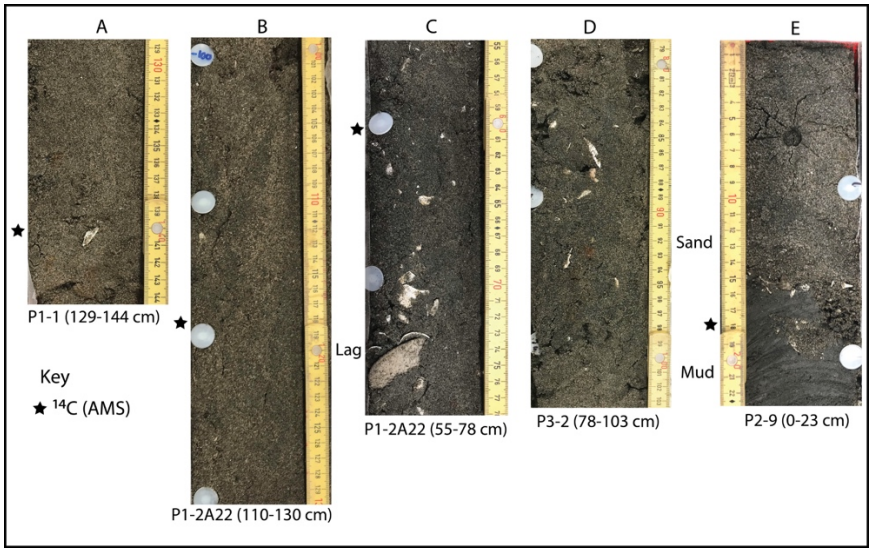

Figure 7. Photographs of selected South PacWave vibracore sections

Vibracore features include: Part A, homogeneous sand in P1-1 at subsurface depth 129–144 cm, Part B, homogenous sand in P1-2A22 at subsurface depth 110–130 cm, Part C, shell and granule lag in sand matrix

support in P1-2A22 at subsurface depth 70–78 cm, Part D, homogenous sand in P3-2 at 78–103 subsurface depth, and Part E, sand/mud contact (disturbed) in P2-9 at 16–18 cm subsurface depth. Star shape imprint in sand at 6 cm depth in P2-9 is from a shear vane (Torvane^{TM}) measurement (not presented in this article).

Unconfined shear strengths were found to be less than 0.25 kg cm^{-2} in vibracores P1-1, P1-2A22, and P3-2 (Table 2, Figure 8), but increased to 0.5–1.5 kg cm^{-2} with increasing depths in vibracores P2-5 and P2-6. The top 10–15 cm of vibracores P2-9 and P3-11 showed low unconfined shear strengths (~0.5 kg cm^{-2}) but underlying sand deposits to ~110 cm depths showed substantial increases in measured unconfined shear strengths (1.5–2.5 kg cm^{-2}). Core sediment colors (moist) vary only slightly from 2.5Y 6/1 to 2.5Y 5/1 (gray) in all cores, except cores P2-9 and P3-11 (Table 2, Figure 8). In those two cores the shallow sandy mud layers (Figure 7) show darker colors, 2.5Y 4/1 to 2.5Y 3/1 (dark gray). The horizontal trends and vertical sequences of these vibracore compositional data are addressed below.

4.2 Lateral Trends and Vertical Sequences of Vibracore Deposits

The South PacWave vibracores show several significant patterns. The first pattern is that of relatively uniform sand grain size (range 0.16–0.28 mm and mean 0.20±0.03 mm 1σ n=18) across the inner-shelf from 19 to 53 m water depth (Table 2). These grain sizes are comparable with 1) the modern beach grain sizes (summer 0.16 ±0.02 mm and winter 0.22±0.02 mm) (Section 2.4) and 2) the inner-shelf surface sample grain sizes (mean ~0.19 mm) reported by Runge (1966) for the PacWave study area. The uniform grain size across the moderately-steep inner-shelf at the PacWave site differs from the broader CRLC inner-shelf areas, where sediment size significantly deceased across the 40–50 m water depth range (Kaminsky, 2006).

The second pattern is apparent in both lateral trends and vertical sequences of increasing unconfined shear strength from <0.25 to >1.5 kg cm^{-2} with increasing distance offshore and with increasing subsurface depths in core sites P2-5, P2-6, P2-9, and P3-11 (Table 2, Figure 8). The greatest unconfined shear strengths (2.25–3.0 kg cm^{-2}) occur in sandy units throughout all but the top 20–30 cm in core sites P2-9 and P3-11 (62–72 m water depth). It is not known whether the high values of unconfined shear strength continue below the shallow subsurface depths of ~ 1 m, as recovered at those two core sites. In the two intermediate depth core sites P2-5 and P2-6, respectively, in 47 and 52 m water depths, unconfined shear strengths increase downcore from 0.25–0.50 to 1.5 kg cm^{-2}. The increases in unconfined shear strength are attributed to sand compaction by wave (cyclic) hydraulic loading with overburden weight over time.

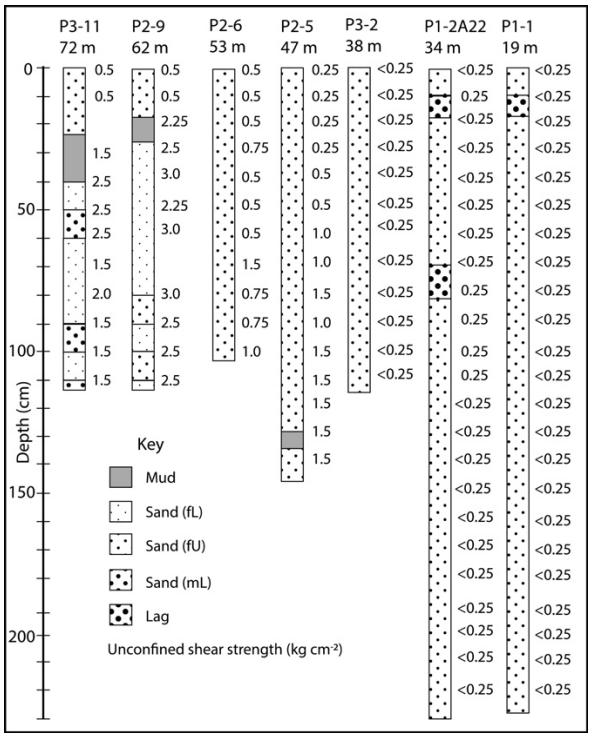

Figure 8. Lateral trends and vertical sequences of South PacWave vibracores

Textures, colors, and unconfined shear strengths (kg cm^{-2}) are from Table 2. Unconfined shear strengths increase both from shallow to deeper water core sites and downcore in the deeper water core sites (P2-5, P2-67, P2-9, and

P3-11). Sand color also darkens slightly in shallow mud layers in core sites P2-9 and P3-11. See Figure 5 for vibracore sites in the PacWave study area.

4.3 Heavy-Mineral Tracers of Sand Sources

Heavy-mineral analyses of potential sand sources (Figure 1) supplied to the South PacWave vibracores are shown in Table 3. Outer-shelf sand deposits are identified by high ratios of metamorphic amphiboles to augite, as represented by the distant Coquille River (MetaAmph:Augite=1.4). Proximal river sand sources include the large antecedent Umpqua River (Hypersthene:Augite=0.9) and local rivers draining the central Coast Range, as represented by the Alsea River (Hypersthene:Augite=0.0). Mixtures of these sand sources supplied 1) the late-Pleistocene dune sheets that crossed the middle and inner-shelf during low-stand conditions, as represented by the Newport Sea Cliff (Hypersthene:Augite=0.7, MetaAmph:Augite=0.5) and 2) the modern beaches, such as at South Beach, located near the Yaquina Bay south jetty (Hypersthene:Augite=0.5, MetaAmph:Augite=0.2) and at Seal Rock beach (Hypersthene:Augite=0.3, MetaAmph:Augite=0.1) (Figure 5). Like the late-Pleistocene dune sheet and the modern beaches, the South PacWave vibracore deposits contain elements from all three sand sources (Figure 9). These sources include the Umpqua River, the local Coast Range rivers, and the outer shelf (Coquille River proxy). The shallower-water vibracore sites (P1-1, P1-2A22, and P3-2) contain slightly larger contributions of sand from the local rivers draining the central Coast Range, relative to Umpqua River sand. The deeper-water core sites (P2-6, P2-9, and P3-11) contain slightly larger contributions of Umpqua River sand relative to central Coast Range rivers. These results are interpreted as follows: the shallow vibracore sites were supplied by modern beach (littoral sand), whereas the deeper vibracore sites appear to reflect sand sources from the Umpqua River and the late-Pleistocene dune sheet in the mid-shelf, which were remobilized and redeposited by the Holocene marine transgression (Section 2.3, Figure 4).

Table 3. Heavy-mineral tracers of sand supply sources to the South PacWave vibracores

Sources and sinks (vibracore #)	Subsurface depth (cm)	Hypersthene:Augite ratio	MetaAmph:Augite ratio
Coquille River	modern	0.2	1.4
Umpqua River	modern	0.9	0.2
Alsea River	modern	0.0	0.0
Newport Sea Cliff	700 cm	0.7	0.5
South Beach	modern	0.5	0.2
Seal Rock Beach	modern	0.3	0.1
South PacWave Cores			
P1-1	100	0.4	0.2
P1-2A22	50	0.4	0.1
P1-2A22	100	0.5	0.1
P1-2A22	150	0.5	0.2
P1-2A22	200	0.5	0.2
P3-2	10	0.4	0.2
P3-2	50	0.4	0.1
P3-2	100	0.3	0.2
P2-5	10	0.3	0.2
P2-5	100	0.7	0.3
P2-6	50	0.8	0.3
P2-9	10	0.6	0.2
P2-9	50	0.8	0.3
P3-11	10	0.8	0.3

Notes: River sand sources include the 1) Coquille River modern deposit (UTM-N 4775000), representing the metamorphic province of the Southern Oregon Coast Range (Figure 1) and the outer shelf in the PacWave study area (Figure 4), 2) Umpqua River modern deposit (UTM-N 4835600), representing the intermediate volcanic province of the Oregon Cascade Range and the mid-shelf in the PacWave study area (Figure 4), 3) Alsea River modern deposit (UTM-N 4919200), representing mudstone and basalt provinces of the Central Oregon Coast

Range, 4) Newport Sea Cliff late-Pleistocene deposit (UTM-N 4929650), representing late-Pleistocene dune sheet deposits in sea cliffs of the PacWave study area (Figure 5), and 5) South Beach modern beach sand (UTM-N 4939500) and Seal Rock modern beach sand (UTM-N 4930650), representing modern beach sand in the PacWave study area. South PacWave inner-shelf vibracores (P-) (Figure 5, Table 1) include representative samples from subsurface depths (cm). Non-opaque minerals include 1) pyroxenes (hypersthene and augite) and 2) metamorphic amphiboles (MetaAmph) (blue-green hornblende, actinolite, and tremolite) (Peterson et al., 2020a). Sand source mineralogy compositions are from Peterson and Kingen (2021).

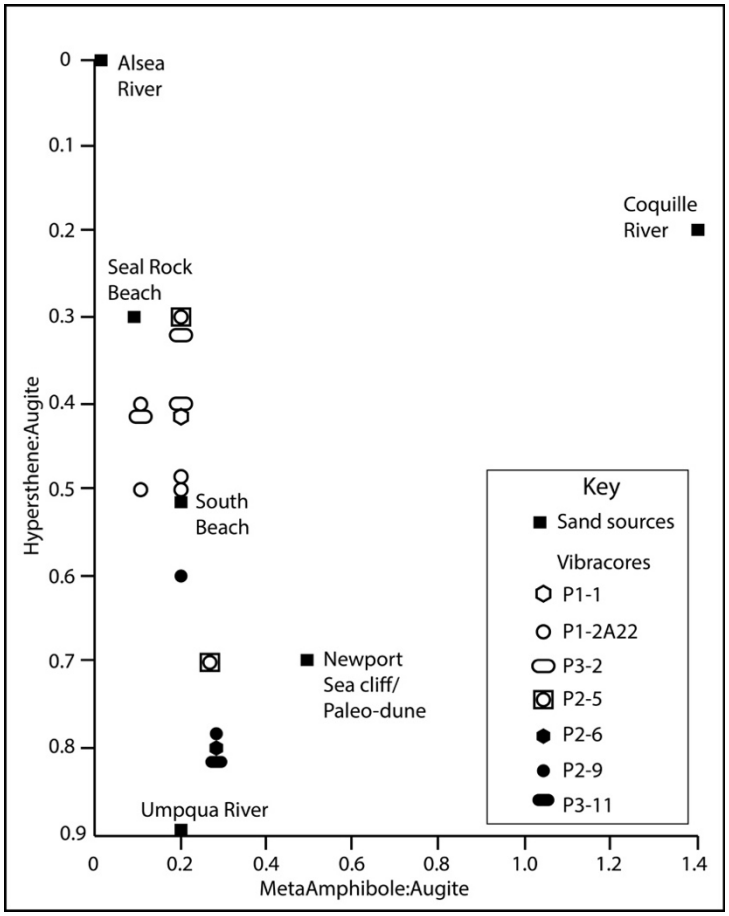

Figure 9. Heavy-mineral tracers of sand sources in South PacWave vibracores

South PacWave vibracores demonstrate compositions that reflect mixtures of sand sources including 1) modern beach (littoral) sand supplies to the shallow water vibracore sites (open symbols) and 2) mid-shelf/paleo-dune sheet sand sources to the deeper water vibracore sites (solid symbols). See Table 3 for sample heavy-mineral ratios and Table 1 for vibracore positions and water depths.

4.4 Radiocarbon Ages and Sedimentation Rates

A basal ^{14}C shell sample at 140 cm depth subsurface from vibracore P1-1 in 19 m water depth yielded an age of 108–273 cal (Table 4) and a corresponding sedimentation rate of 55 cm century^{-1} (Table 5). Because this rate substantially exceeds relative sea level rise (10 cm century^{-1}) in the study area, it is assumed to represent a significant component of mixing, possibly by resuspension and deposition in the innermost-shelf site. A shallow sample from vibracore P1-2A22 at 60 cm subsurface depth returned a modern age (conventional 920±30, 390±29 delta-R), which is invalid for MARINE20 calibration. This 'modern' shell age indicates a near-modern mixing depth of at least 60 cm for the P1-2A22 site in 34 m water depth. Mid-core ^{14}C shell samples from vibracore P1-2A22 at 118 cm and 178 cm subsurface depths, respectively, yielded ages of 606–670 cal and 565–574 cal, and corresponding sedimentation rates of 17 cm century^{-1} and 31 cm century^{-1}. The similar ages at 118 and 178 cm subsurface depth attest to a paleo-mixing depth of at least 60 cm during that prehistoric interval. Assuming mixing values of 60–100 cm at 34 m water depth, the calculated sedimentation rates are interpreted to yield approximate net sedimentation rate(s) that exceed coeval SLR of 10 cm century^{-1}, as discussed below in Section 5.2. A near basal ^{14}C shell sample from 87 cm subsurface depth from vibracore P3-2 in 38 m water depth

yielded a modern age, indicating a modern mixing depth of at least 87 cm subsurface depth. A shallow ^{14}C shell sample at 35 cm subsurface depth from vibracore P2-5 in 47 m water depth yielded a near modern age, so it is interpreted to represent a mixing depth of at least 35 cm for that site. The basal sand deposits at 87 cm depth subsurface in vibracore P2-6 in 53 m water depth are of early-Holocene age 10,046–10,4212 cal (Table 4). The basal sand deposits (110 cm depth subsurface) in vibracore P2-9 in 62 m water depth also dated to earliest-Holocene time 10,391–10,812 cal. Basal contacts from two thin sand units above anomalous mud layers in P2-9 and P3-11 (Figure 7E), respectively, date to the early- to mid-Holocene marine transgression: 9,890–10,235 cal and 12,760–12,903 cal.

Early Holocene deposits P2-6 and P2-9 (Table 3) are associated with significantly compacted sand (>0.75 kg cm^{-2}) and heavy-mineral tracer indicators of early- to mid-Holocene transgressive sand supply (Table 2). The relative compaction (unconfined shear strength) of basal sand deposits in the South PacWave vibracores provides relative dating constraints on the duration of deposit emplacement. For example, all the intervals to subsurface depths of 110 cm in vibracore P3-2 in 38 m water depth show negligible compaction (unconfined shear strength ≤0.25 kg cm^{-2}), indicating late-Holocene ages of emplacement. However, basal sand samples, at ≥80 cm depth subsurface in P2-5 show substantial compaction (1.5 kg cm^{-2}). Using a presumed transgressive surface age of at least 9 ka for the subsurface depth interval at 80–100 cm in vibracore P2-5 in 47 m water depth (Figure 2D) yields a proxy sedimentation rate of 0.9 cm $century^{-1}$.

Table 4. ^{14}C ages of deposits in the South PacWave vibracores

Sample ID	Material	Conventional (yr)	Delta-R (yr)	Calibrated (cal)	Lab ID
P1-1VC-140 cm	shell	1,120±30	390±29	108-273*	Beta-620446
P1-2A22VC-60 cm	shell	9200±30	390±29	modern	Beta-620447
P1-2A22VC-118 cm	shell	1,510±30	390±29	606-770	Beta-565636
P1-2A22VC-178 cm	shell	1500±30	390±29	565-754	Beta-565637
P3-2VC-87 cm	shell	790±30	390±29	modern	Beta-620449
P2-5VC-35 cm	shell	1,100±30	390±29	modern	Beta-620450
P2-6VC-87 cm	shell	9,920±30	390±29	10,046-10,4212	Beta-616362
P2-9VC-18 cm	shell	9,810±30	390±29	9,890-10,235	Beta-616364
P2-9VC-110cm	shell	10,210±30	390±29	10,391-10,812	Beta-616363
P3-11VC-25cm	wood	10,940±30	-	12,760-12,903	Beta-616365

Notes: AMS ^{14}C ages in years BP include conventional (yr) and calibrated (cal) at 95.4 % probability (2 σ) by local marine reservoir correction (Delta-R) and BetaCal 4.20 using MARINE20 (Heaton et al., 2020). *Calibrated sample ages for 1 σ (68% probability) using MARINE20 (Calib8.20) (Stuiver et al., 2022). Lab ID numbers are from Beta Analytic Inc. See Table 1 for positions and water depths of the South PacWave vibracores. The radiocarbon ages are plotted in core logs with corresponding deposit textures and depths in Figure 10 (Section 5.1).

Table 5. Sedimentation rates in South PacWave vibracores

Vibracore/ ^{14}C sample depth (cm)	Depth interval (cm)	Age interval (yr)	Sedimentation rate (cm $century^{-1}$)
P1-2A22 (118)	118	690	17
P1-2A22 (178)	178	570	31
P2-5 (80) †	80	9,000	0.9†
P2-6 (87)	87	10,000	0.9

Notes: Sedimentation rates are based on depth intervals (cm) divided by age (yr) taken to be the mid-point of the reported calibrated ages (Table 4), as normalized to cm per century (cm $century^{-1}$). †A proxy age of early

Holocene age (9 ka) is assigned to P2-5 at 80 cm depth, based on an unconfined shear strength (1.5 kg cm^{-2}) and nearest sample (P2-5 100 cm depth) mineralogy of early transgressive sand supply (Table 3).

5. Discussion

5.1 Inner-shelf Facies

Shallow deposits of littoral sand (≥1.0 m thickness) extend across the inner-shelf to water depths of ~40 m in the South PacWave study site (Figure 10). The inner-shelf distributions of sand grain sizes (mean 0.20±0.03 mm 1σ n=18) (Section 4.1) are consistent with sand supply from littoral sand sources, as identified by heavy-mineral tracers (Section 4.3). Coarser lag deposits of shell fragments and rare pebbles (<1.0 cm diameter) are generally thin (~1–3 cm thickness), but thicker lag deposits (≥5 cm thickness) occur in core sites to water depths of 34 m. Pebbles >1.0 cm in diameter were generally absent from the thin lag layers in vibracores from sites deeper than 34 m water depth. Unconfined shear strength (Section 4.2), heavy-mineral tracer data (Section 4.3), and ^{14}C dating (Section 4.4) all show that sandy facies in the South PacWave site represent two very different origins. The shallower vibracores P1-1, P1-2A22, and P3-2 (19–38 m water depth) contain late-Holocene deposits, representing seaward transport and deposition of littoral sand during post-transgressive conditions of near high-stand (Figure 10B; Figure 2D). A possible transition from late-Holocene to early-Holocene age occurs across the subsurface depth interval of 60–80 cm in P2-5 (see Section 4.4). The deeper vibracores P2-6, P2-9, and P3-11 (53–72 m water depth) all contain early-Holocene deposits, representing reworking and deposition of mid-shelf deposits during the early-Holocene marine transgression (≥10 ka). The similarity in sand grain-size across the inner-shelf is due to fine-sand sources from 1) mudstones in local tributary drainages (Peterson et al, 1982), 2) large dune sheets that crossed the continental shelf during late-Pleistocene time (Peterson et al., 2007), and 3) bypassing of river sand through small estuaries in late-Holocene time (Section 2.3). The earliest-Holocene ages in the deeper core sites (P2-6, P2-9, and P3-11) reflect an abandonment of sand supply to those sites, following the coeval Holocene marine transgression across the mid-shelf (Figure 2D). The origin(s) of thin sand units above the anomalous mud layers in vibracores P2-9 and P3-11 (Table 2 and Figure 10) are unknown at present time, but they warrant further study.

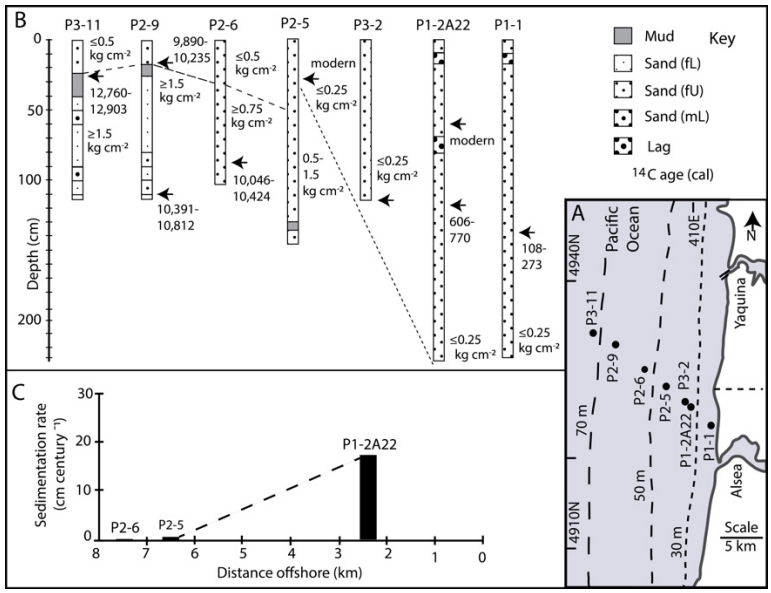

Figure 10. Stratigraphic correlations and sedimentation rates in South PacWave vibracores

Part A, Map of vibracore sites in the South PacWave study site. Part B, ^{14}C radiocarbon ages and stratigraphic correlation of vibracore logs. Part C, plot of sedimentation rates (cm century^{-1}) relative to across-shelf distance (km) in the South PacWave study site. Radiocarbon ages are from Table 4. Sedimentation rates are from Table 5. Interpreted stratigraphic correlations (dashed lines) in Part B are based on unconfined shear strengths (Table 2). Low shear strengths (above dotted line) are associated (correlated) with latest-Holocene (young) deposits in vibracores P1-1, P1-2A22, P3-2 and P2-5. High shear strengths (below dashed line) are associated (correlated) with earliest-Holocene (old) deposits in vibracores P2-6, P2-9, and P3-11.

5.2 Depths of Closure in the South PacWace Study Area

Offshore annual disposals of dredged material (fine sand) from the harbor areas of Yaquina Bay (Figure 5) have averaged 1.5–2.0x10^5 m^3 yr^{-1} (USACE, 2012). To minimize material haul costs a variety of inner-shelf sites, ranging from ~20 to ~50 m water depths, were utilized for offshore disposal. Longshore movements of sand are reduced between shallow rocky-reefs (15–30 m water depth), located to the northwest and southwest of the Yaquina Bay entrance. A small interim disposal site (~20 m water depth) between the rocky-reefs was utilized for dredged material disposal (1977–1985). Mounds of disposed material required multiple stormy winters to degrade or disperse to flat seabed conditions (S. A. Chesser, US Army Corps of Engineers, Portland District, pers. comm, 1987). Subsequent disposal at deeper sites (25–30 m water depths) produced mounds that did not fully degrade during the next decade (USACE, 2012). The results above suggest a ~20 m depth of closure, or depth of across-shelf mixing, at the decadal time scale, in the PacWave study area.

Different methods can be used to establish longer-period depth(s) of closure in the high-energy PNW region, including the use of littoral sand sedimentation rates, as measured at different water depths across the inner-shelf (Sections 4.1 and 4.2). A proxy depth of closure (30 m water depth for a one century interval) for different scenarios of possible future SLR in the PNW study region have been proposed, based on comparisons of sedimentation rates and coeval rates of SLR in the CRLC study area (Figure 3) (Peterson et al. 2020a; Peterson et al., 2020b). The ages of sand emplacement in the inner-shelf of the South PacWave study site are complicated by recent deposit resuspension and deposition, or mixing by overturning. For example, modern or near modern ^{14}C shell fragment ages occur at subsurface depths of 140, 60, 87, and 35 cm, respectively, in vibracores P1-1, P1-2A22, P3-2, and P2-5 (Table 4). The depths of recent mixing generally decrease across the inner-shelf from >1.4 m subsurface depth in P1-1 in 19 m water depth to < 20 cm subsurface depth in P2-9 in 62 m water depth (Table 4). The decrease in mixing depth across the inner-shelf is assumed to reflect decreasing wave bottom orbital energy and/or entrainment resuspension velocities with increasing water depths. ^{14}C dated deposits from vibracores that significantly exceed the near modern mixing depths are assumed to provide approximate net sedimentation rates. In vibracore P1-2A22, two calculated sedimentation rates (17 cm $century^{-1}$ and 31 cm $century^{-1}$) (Table 5) are assumed to represent net sedimentation rates that equal or exceed coeval relative SLR (10 cm $century^{-1}$), when adjusted for likely mixing depths (60–100 cm). The short vibracore length (110 cm) recovered from P3-2 might not extend significantly below modern mixing depth (at least 87 cm subsurface), so it is not suitable for estimating net-sedimentation rates during latest-Holocene time. Longer vibracore lengths (≥2.5 m) in the vicinity of P3-2 are required to establish whether multi-century depths of closure do reach 38 m water depth in the South PacWave study site. The ~1.0 m vibracore lengths from the mid-shelf water depths (> 50 m) at the South PacWave study site are suitable for establishing late-Holocene sedimentation rates. The very low sedimentation rates in P2-5 and P2-6 (Table 5) are well below any significance for depth of closure in late-Holocene time.

5.3 Implications of Littoral Sand Displacements

There should be growing concern about potential impacts from future SLR in the PNW study region (Figure 1) and in other high-energy coastlines worldwide. One such impact is the offshore displacement of littoral sand to fill increasing accommodation space across the innermost-shelf (Sections 2.1 and 2.2), following predicted future SLR (≥1.0 m) (Horton et al., 2020). During the latest-Holocene time littoral sand has accumulated to >1.0 m thickness across the inner-shelf to water depths of at least 38 m (Table 3, Figure 10). Even with beach sand feeding from small rivers and sea cliff erosion, the relatively large sink of littoral sand in the inner-shelf explains the net erosion of northern Oregon beaches during latest-Holocene time (Section 2.3) (Peterson et al., 2019). If littoral sand were to be displaced across the innermost-shelf (5–30 m water depth) following a near future (one century) SLR or increased accommodations space of 1.0 m, then a cross-sectional area of ~1.5x10^3 m^2 would be required to fill the increased accommodation space below wave base. But that value is three times greater than the average cross-sectional area (mean ~4.8x10^2 m^2, n=11) of the existing beaches in the PacWave study area (Peterson and Kingen, 2021). The loss of beach sand to fill the offshore accommodation space would erode the sandy beaches and expose intertidal wave-cut platforms in front of retreating or artificially stabilized sea cliffs. The resulting intertidal platforms (bedrock) could become locally covered by beach gravel, algae, and/or invertebrates. The popular sandy beaches of the northern Oregon coast (Figure 4) would largely cease to exist (Peterson et al., 2021).

5.4 Comparisons with Other PNW Study Areas

The latest-Holocene depth of closure in the PacWave study area (Figure 10) supports the proposed depth of closure (≥30 m) in the moderately-steep innermost-shelf of the Gold Beach study area (Figure 2 in Section 2.1).

Southward transport of Rogue River sand filled both the nearshore and innermost-shelf in the Gold Beach study area (to at least 30 m water depth) to keep pace with SLR (1.0 m ka^{-1}) during late-Holocene time (Figure 2). The net seaward transport of littoral sand during late-Holocene time is demonstrated by mineralogical evidence that shows that the sand fill originated from the large antecedent Rogue River and not the mid- or outer-shelf. The Rogue River delivers bedload (~$0.7x10^6$ m^3 yr^{-1}) to the adjacent beaches in the Gold Beach study area (average width 160±49 m 1σ, n=6), which has maintained most of the adjacent beaches with little to no recent sea cliff retreat. However, the southward net longshore transport and the filling of the inner-shelf accommodation space has precluded significant beach progradation in the Gold Beach area in late-Holocene time. Because net longshore transport carries some of the Rogue River sand well south (>10 km) of the Gold Beach study area (Figure 2), the Gold Beach study area could lose substantial beach sand widths to offshore sand displacement following predicted future SLR (Peterson et al., 2021). The PacWave study area (Figures 4 and 5) lacks strong net longshore transport, but it also lacks a large river sand supply (Section 2.4). An offshore displacement of littoral sand, like in the Gold Beach study area, did keep pace with very latest-Holocene SLR across the inner-shelf in the PacWave study area (Figure 10). The long-term seaward transport of littoral sand in the PacWave study area, without substantial river sand supply, caused the long-term thinning and narrowing of adjacent beach deposits in latest-Holocene time (Peterson et al., 2019).

Very-large retreat scarps in the CRLC system (Figure 3 in Section 2.2) required very-large displacements of littoral sand across the innermost-shelf, following abrupt coseismic subsidence events (abrupt SLR 1±0.5 m). Such displacements occurred in <70-year time scales (Figure 3). Over longer time scales (multi-century), across-shelf transport of littoral sand reached 30–40 m water depths or 5–8 km distance offshore in the CRLC system. Were such across-shelf sand displacements influenced by the very large seasonal discharges of the Columbia River, or by large ebb-tidal deltas, or by the large coseismic subsidence events in that region? It was not known whether the long-term across-shelf transport of littoral sand to 30–40 m water depth in the CRLC system was representative of other PNW coastal settings. The South PacWave site shows that across inner-shelf transport of littoral sand did occur to 30–40 m water depth during late-Holocene time (Figure 10), but without the presence of 1) large river discharge, 2) large ebb-tidal deltas, 3) large projecting headlands, and/or 4) large magnitudes of coseismic subsidence (Section 2.4). Observations of modern nearshore sand transport and assumed depths of closure in some PNW localities are not sufficient to address potential impacts of prolonged near future SLR. Century time scale depths of closure need to be established from empirical measurements of littoral sand accumulation rates in different inner-shelf settings. No records of coseismic (pre-historic) beach retreat are recorded in the narrow (eroded) PacWave beaches. However, the potential for such displacements to occur under near future (one century) conditions of SLR are demonstrated by the preserved ^{14}C dated geologic records of displacements (< 1.0 century) that did follow coseismic subsidence events, as recorded in the net prograded barriers and beach plains of the nearby CRLC system (Peterson et al., 2010).

5.5 Possible Mechanisms of Bottom Current Transport Across PNW Inner-shelf Settings

Across inner-shelf transport of littoral sand in the low-gradient CRLC system (Figure 3) has been modeled using combined oscillatory resuspension and geostrophic flow forced by storm winds and waves (Kachel and Smith, 1986; Sternberg, 1986). Mud transport to the mid-shelf offshore of the Eel River, about 200 km south of the Gold Beach study area (Figure 1), has been related to density-driven bottom flows during major storm events (Cacchione et al., 1999; Traykovski et al., 2000; Ogston et al., 2004). It is not known what combination(s) of hydrodynamic processes might account for the transport of littoral sand across the inner-shelf in the PacWave study area. The substantial decrease in sedimentation rate between P3-2 and P2-5 coincides with a substantial decrease in inner-shelf gradient between the two vibracore sites (Figure 10). However, the abrupt decreases in littoral sand sedimentation rates seaward of the ~40 m water depth in both the CRLC system (Figure 3) and the PacWave study area (Figure 10) suggest that depth(s) of closure in the PNW region are controlled by maximum effective depths of oscillatory bottom current resuspension, or peak wave base.

What specific conditions of 1) oscillatory bottom current resuspension, 2) unidirectional bottom current entrainment, 3) shelf bathymetry, and/or 4) littoral sand size and abundance control the depth(s) of closure in the high-energy settings of the PNW region? A better understanding of the relations that control the depth of closure in high-energy coastal settings will require long-term monitoring for the unique wave, wind, shelf bathymetry, and grain size conditions that can episodically transport littoral sand across the inner-shelf. For example, a semi-permanent offshore mooring, power, and data transfer system could be supplied by the South PacWave wave-energy testing facility in northern Oregon (Figure 5) (PacWave, 2022). Long-term measurements of wave, wind, bottom currents, and sediment transport in different water depths from such facilities could establish and/or verify needed modeling parameters in helping to predict beach sand displacements from future SLR.

However, empirical measurements of littoral sand accumulations across inner-shelves that have experienced recent SLR provide immediately available constraints on depths of closure for predicting potential beach erosion impacts from future SLR.

6. Conclusions

The Pacific Northwest (PNW) study region provides the necessary conditions to study depth(s) of closure in high-energy inner-shelf settings, including high wave- and wind-energies and both short-term (cyclic) and long-term (net) events of sea level rise (SLR). However, variable conditions of 1) littoral sand size and abundance, 2) longshore transport, and 3) inner-shelf bathymetry require different site evaluations to establish the relative importance's of these variables in controlling measured depth(s) of closure. The PacWave study area, in the central part of the PNW study region, is characterized by high wave-energy, a relatively steep innermost-shelf gradient, and low abundance(s) of littoral sand supply. Very-latest-Holocene (≤1.0 ka) depth of closure reaches at least 34 m water depth in the South PacWave study site but not in deeper water depths of 47–53 m. Such constraints on depth of closure are needed to calculate inner-shelf widths of littoral sand accommodation space. Increasing inner-shelf accommodation space, following relative SLR, leads to offshore displacements of beach sand and ensuing beach erosion. Locally variable conditions of river sand throughput, longshore transport, and/or sand supply from sea cliff erosion can also influence net erosion of beaches and/or beach recovery. But low rates of littoral sand supply in the PacWave study area were insufficient to maintain beach widths following the last 1.0 m increase in sea level rise during latest-Holocene time. No significant resupply of beach sand is expected to occur in the South PacWave area during the much shorter period (~100 years) of catastrophic beach erosion following predicted near future SLR. The study methods that are reported here should have broad relevance to other high-energy coastlines worldwide that face catastrophic beach sand erosion from predicted near-future SLR. Long-term monitoring of inner-shelf wave, wind, and bottom current conditions in offshore monitoring facilities, such as at the South PacWave study site, are proposed to establish the specific, and possibly infrequent, conditions that lead to transport and deposition of littoral sand across the inner-shelf in high-energy coastal settings. However, empirical methods of measuring recent littoral sand transport and net accumulation across inner-shelf settings provide the most direct, and immediately available, constraints on depth(s) of closure in high-energy coastal settings.

Acknowledgements

Maziet Cheseby provided access to archived PacWave vibracores, core site data, and laboratory workspace in the Marine Geology Repository at Oregon State University. This article benefited from an early review by Kara Kingen. Kennett Peterson assisted with early manuscript editing. Support for the archival of, and access to, the PacWave vibracores in the Marine Geology Repository at Oregon State University (OSU-MGR-NSF) was provided by the National Science Foundation under Grant number OCE-1558679.

References

Bamber, J. L., Oppenheimer, M., Kopp, R. E., Aspinall, W. P. & Cooke, R. M. (2019). Ice sheet contributions to future sea-level rise from structured expert judgment. *Proceedings of the National Academy of Sciences, 116*, 11195-11200. https://doi.org/10.1073/pnas.1817205116

Bruun, P. (1962). Sea-level rise as a cause of shore erosion. *Journal of the Waterways and Harbors Division, 88*, 117-132. https://doi.org/10.1061/JWHEAU.0000252

Bruun, P. (1988). The Bruun rule of erosion by sea-level rise: a discussion on large-scale two-and three-dimensional usages. *Journal of Coastal Research, 4*, 627-648.

Cacchione, D. A., Wiberg, P. L., Lynch, J., Irish, J. & Traykovski, P. (1999). Estimates of suspended-sediment flux and bedform activity on the inner portion of the Eel continental shelf. *Marine Geology, 154*, 83-97. https://doi.org/10.1016/S0025-3227(98)00105-4

Clifton, H. E., Connard, G. G., Fisher, J., Fox, D., Mardock, C., McMurray, G., O'Brien, R. J., Peterson, C., Starr, R., & Woolsey, R. (1990). Cruise report 1990 Oregon placer mineral research cruise (Al 90WO) September 21-October 3, 1990. U.S. Geological Survey, Open-File Report 91-279, 81 p.

Clifton, H. E., Peterson, C. D. & Connard. G. (1991). Geology and geophysics, In Preliminary Resource and Environmental Data: Oregon placer minerals, Joint State-Federal Oregon Placer Minerals Technical Task Force, Oregon Department of Geology and Mineral Industries, Open-File Report 0-91-02, 9-74 pp.

Cruikshank, K. M. & Peterson, C. D. (2017). Late-stage interseismic strain interval, Cascadia subduction zone margin, USA and Canada. *Open Journal of Earthquake Research, 6*, 1-34. http ://www.scirp.org/journal/ojer. https://doi.org/10.4236/ojer.2017.61001.

Erikson, L. H., O'Neill, A., Barnard, P. L., Vitousek, S., & Limber, P. (2017). Climate change- driven cliff and beach evolution at decadal to centennial time scales. *Coastal Dynamics, 2017*, 125–136.

Google Earth. (2022). Google Earth. Accessed Janurary 5, 2021. https://www.google.com/earth/

Hamilton, D. M. (1994). Sediment yield analysis of Reservoir #1, Bull Run Watershed, west Cascade mountains, Oregon. M.S. Thesis, Portland State University, Portland, Oregon, 333 p.

Hart**,** R. & Peterson, C. (2007). Late-Holocene buried forests on the Oregon coast. *Earth Surface Processes and Landforms, 32*, 210-229. https://doi.org/10.1002/esp.1393

Heaton, T. J., Köhler, P., Butzin, M., Bard, E., Reimer, R. W., Austin, W. E., Ramsey, C. B., Grootes, P. M., Hughen, K. A., Kromer, B. & Reimer, P. J. (2020). Marine20—the marine radiocarbon age calibration curve (0–55,000 cal BP). *Radiocarbon, 62*, 779-820. https://doi.org/10.1017/RDC.2020.68

Horton, B. P., Khan, N. S., Cahill, N., Lee, J. S., Shaw, T. A., Garner, A. J., Kemp, A. C., Engelhart, S. E. & Rahmstorf, S. (2020). Estimating global mean sea-level rise and its uncertainties by 2100 and 2300 from an expert survey. *Climate and Atmospheric Science, 3*, 1-8. https://doi.org/10.1038/s41612-020-0121-5. https://doi.org/10.1038/s41612-020-0121-5

Kachel, N. B., & Smith, J. D. (1986). Geologic impact of sediment transporting events on the Washington continental shelf. In: Knight, R. J., McLean, J. R. (eds.), *Shelf Sands and Sandstones, Canadian Society of Petroleum Geologists,* Memoir II, p. 145–162.

Kaminsky**,** G. M. (2006). Shoreface Behavior and Equilibrium. Unpublished PhD Thesis University of Sydney, New South Wales, 633 p.

Kaminsky, G. M., Ruggiero, P., Buijsman, M. C., McCandless, D., & Gelfenbaum, G. (2010). Historical evolution of the Columbia River littoral cell. *Marine Geology, 273*, 96-126. https://doi.org/10.1016/j.margeo.2010.02.006

Kulm, L. D. & Byrne, J. V. (1966). Sedimentary response to hydrography in an Oregon estuary. *Marine Geology, 4*, 85-118. https://doi.org/10.1016/0025-3227(66)90001-6

Mardock, C. (1991). Mineralogy and Geochemistry, In Preliminary Resource and Environmental Data: Oregon placer minerals, Joint State-Federal Oregon Placer Minerals Technical Task Force, Oregon Department of Geology and Mineral Industries, Open-File Report 0-91-02, 9-74 pp.

Meyers, R. A., Smith, D. G., Jol, H. M., & Peterson, C. D. (1996). Evidence for eight great earthquake-subsidence events detected with ground-penetrating radar, Willapa barrier, Washington. *Geology, 24*, 99-102. https://doi.org/10.1130/0091-7613(1996)024<0099:EFEGES>2.3.CO;2

Ogston, A. S., Guerra, J. V. & Sternberg, R. W. (2004). Interannual variability of nearbed sediment flux on the Eel River shelf, northern California. *Continental Shelf Research, 24*, 117-136. https://doi.org/10.1016/j.csr.2003.08.007

PacWave. (2019). Vibracore Logs from Research Cruise MSL1903 (pdf). College of Engineering, Oregon State University, Corvallis, Oregon. 27 p.

PacWave. (2022). PacWave Testing Wave Energy for the Future. PacWave Energy.org. Accessed February 1, 2022. https://pacwaveenergy.org

Peterson**,** C. D., Carver, G. A., Clague, J. J., & Cruikshank, K. M. (2015). Maximum-recorded overland run-ups of major nearfield paleotsunamis during the past 3,000 years along the Cascadia margin, USA and Canada. *Natural Hazards, 77*, 2005-2026. https://doi.org/10.1007/s11069-015-1689-7

Peterson, C. D., Doyle, D. L., & Barnett, E. T. (2000). Coastal flooding and beach retreat from coseismic subsidence in the central Cascadia margin, USA. Environmental and *Engineering Geology, 6*, 255-269. https://doi.org/10.2113/gseegeosci.6.3.255

Peterson**,** C. D., Doyle, D. L., Rosenfeld, C. L., & Kingen, K. E. P. (2020a). Predicted responses of beaches, bays, and inner-shelf sand supplies to potential sea level rise (0.5-1.0 m) in three small littoral subcells in the high-wave-energy Northern Oregon Coast, USA. *Journal of Geography and Geology, 12*, 1-27. https://doi.org/10.5539/jgg.v12n2p1

Peterson, C. D., Jol, H. M., Woxell, L.K., Vanderbugh, S., Phipps, J., Percy, D., Reckendorf, F. & Gelfenbaum, G. (2002). Late-Holocene shoreface retreat scarps from ground penetrating radar profiles: Columbia River littoral cell, Washington-Oregon, USA. Department of Geology Open File Report, Portland State University, Portland, Oregon. 78 GPR profile section (gif) images.

Peterson, C. D., Jol., H. M., Vanderburgh, S., Phipps, J. B., Percy, D., & Gelfenbaum, G. (2010). Dating of late-Holocene shoreline positions by regional correlation of coseismic retreat events in the Columbia River littoral cell. *Marine Geology, 273*, 44-61. https://doi.org/10.1016/j.margeo.2010.02.003

Peterson, C. D., & Kingen, K. E. P. (2021). Pacific Northwest Littoral Data. Dataset. https://doi.org/10.15760/geology-data.01. Accessed January 8, 2022.

Peterson, C. D., Kingen, K. E., Erlandson, J. M., Kaijankoski, P., Meyer, J. & Ryan, C. (2019). Widespread evidence of terminated marine transgressive sand supply and failing longshore sand transport to eroding coastal eolian sand ramps during the latest Holocene time in Oregon and California (Pacific Coast, USA). *Journal of Coastal Research, 35*, 1145-1163. https://doi.org/10.2112/JCOASTRES-D-19-00013.1

Peterson**,** C. D., Linde, T. C. & Vanderburgh, S. (2020b). Late-Holocene Shoreline Responses To Competing Shelf, Bay, and Beach Accommodation Spaces Under Conditions of Relative Sea Level Change And The Potential for Future Catastrophic Beach Retreat In The Columbia River Littoral Cell, Washington and Oregon, USA. *Marine Geology, 24*, Published online. https://doi.org/10.1016/j.margeo.2020.106272.

Peterson, C. D., Pettit, D. J., Kingen, K. E. P., Vanderburgh, S., & Rosenfeld, C. L. (2021). Catastrophic beach sand losses due to erosion from predicted future sea level rise (0.5–1.0 m), based on increasing submarine accommodation spaces in the high-wave-energy coast of the Pacific Northwest, Washington, Oregon, and Northern California, USA. *Marine Geology, 439*, Published Online 2021, 106555. https://doi.org/10.1016/j.margeo.2021.106555

Peterson, C. D., Scheidegger, K. F. & Komar, P. D. (1982). Sand dispersal patterns in an active- margin estuary of the northwestern United States as indicated by sand composition, texture and bedforms. *Marine Geology, 50*, 77-95. https://doi.org/10.1016/0025-3227(82)90062-7

Peterson, C. D., Stock, E., Hart, R., Percy, D., Hostetler, S. W., & Knott, J. R. (2009). Holocene coastal dune fields used as indicators of net littoral transport: West Coast, USA. *Geomorphology, 116*, 115-134. https://doi.org/10.1016/j.geomorph.2009.10.013

Peterson, C. D., Stock, E., Price, D. M., Hart R., Reckendorf, F., Erlandson, J. M., & Hostetler, S. W. (2007). Ages, distributions, and origins of upland coastal dune sheets in Oregon, USA. *Geomorphology, 91*, 81-102. https://doi.org/10.1016/j.geomorph.2007.02.005

Peterson, C. D., Twichell, D. C., Roberts, M. C., Vanderburgh, S., & Hostetler, S. W. (2016). Accommodation space in a high-wave-energy inner-shelf during the Holocene marine transgression: correlation of onshore and offshore inner-shelf deposits (0–12 ka) in the Columbia River littoral cell system, Washington and Oregon, USA. *Marine Geology, 379*, 140-156. https://doi.org/10.1016/j.margeo.2016.05.007

Priest, G. R. & Allan, J. C. (2004). *Evaluation of coastal erosion hazard zones along dune and bluff backed shorelines in Lincoln County, Oregon: Cascade Head to Seal Rock*. Oregon Department of Geology and Mineral Industries, Coastal Field Office. p 79.

Rosen, P. S. (1978). A regional test of the Bruun Rule on shoreline erosion. *Marine Geology, 26*, 7-16. https://doi.org/10.1016/0025-3227(78)90052-X

Runge, E. J. (1966). Continental shelf sediments, Columbia River to Cape Blanco, Oregon. Ph.D. thesis. Oregon State University, Oregon, 143 p.

Scheidegger, K. F., Kulm, L. D., & Runge, E. J. (1971). Sediment sources and dispersal patterns of Oregon continental shelf sands. *Journal of Sedimentary Petrology, 41*, 1112–1120. https://doi.org/10.1306/74D72414-2B21-11D7-8648000102C1865D

Sherwood, C. R., Jay, D. A., Harvey, B., Hamilton, P. & Simenstad, C.A. (1990). Historical changes in the Columbia River estuary. *Progress in Oceanography, 25*, 299-352. https://doi.org/10.1016/0079-6611(90)90011-P

Sternberg, R. W. (1986). Transport and accumulation of river-derived sediment on the Washington continental shelf, USA. *Journal of the Geological Society, London, 143*, 945–956. https://doi.org/10.1144/gsjgs.143.6.0945

Stuiver, M., Reimer, P. J., & Reimer, R. W. (2022). CALIB 8.2 [WWW program] at http://calib.org, accessed March 8, 2022. http://calib.org/calib/calib.html.

Traykovski, P., Geyer, W. R., Irish, J. D., & Lynch, J. F. (2000). The role of wave-induced density-driven fluid mud flows for cross-shelf transport on the Eel River continental shelf. *Continental Shelf Research, 20*, 2113–2140. https://doi.org/10.1016/S0278-4343(00)00071-6

Twichell**,** D. C., Cross, V., & Peterson, C. D. (2010). Partitioning of sediment on the shelf offshore of the Columbia River littoral cell. *Marine Geology, 273*, 11-31. https://doi.org/10.1016/j.margeo.2010.02.001

USACE. (2015). Environmental Assessment Yaquina Bay and River Maintenance Dredging. U.S Army Corps of Engineers, Portland District and Moffatt and Nichol, Seattle Washington. 91 p. p16021coll7_2679.pdf. https://usace.contentdm.oclc.org. Accessed January 13, 2022.

USACE. (2012). Yaquina Bay, Oregon Ocean Dredged Material Disposal Sites Evaluation Study and Environmental Assessment. U.S Army Corps of Engineers, Portland District and U.S. Environmental Protection Agency Region 10. https://tethys.pnnl.gov/sites/default/files/publications/EPA-R10-OW-2012-0197-0043.pdf. Accessed February 2021. https://tethys.pnnl.gov/publications/yaquina-bay-oregon-ocean-dredged-material-disposal-sites-evaluations-study.

Woxell, L. K. (1998). Prehistoric beach accretion rates and long-term response to sediment depletion in the Columbia River littoral cell. M.S. Thesis, Portland State University, Portland, Oregon, 206 p.